



Article

Polysiloxane-Based Polyurethanes with High Strength and Recyclability

Wencai Wang^{1,2,3}, Xueyang Bai¹, Siao Sun¹, Yangyang Gao^{1,2,3} , Fanzhu Li^{1,2,3,*} and Shikai Hu^{1,2,3,*}

¹ State Key Laboratory of Organic-Inorganic Composites, Beijing University of Chemical Technology, Beijing 100029, China

² Key Laboratory of Carbon Fiber and Functional Polymers, Ministry of Education, Beijing University of Chemical Technology, Beijing 100029, China

³ Beijing Engineering Research Center of Advanced Elastomers, Beijing University of Chemical Technology, Beijing 100029, China

* Correspondence: lifz@mail.buct.edu.cn (F.L.); skhu@mail.buct.edu.cn (S.H.)

Abstract: Polysiloxanes have attracted considerable attention in biomedical engineering, owing to their inherent properties, including good flexibility and biocompatibility. However, their low mechanical strength limits their application scope. In this study, we synthesized a polysiloxane-based polyurethane by chemical copolymerization. A series of thermoplastic polysiloxane-polyurethanes (Si-TPUs) was synthesized using hydroxyl-terminated polydimethylsiloxane containing two carbamate groups at the tail of the polymer chains 4,4'-dicyclohexylmethane diisocyanate (HMDI) and 1,4-butanediol as raw materials. The effects of the hard-segment content and soft-segment number average molecular weight on the properties of the resulting TPUs were investigated. The prepared HMDI-based Si-TPUs exhibited good microphase separation, excellent mechanical properties, and acceptable repeatable processability. The tensile strength of SiTPU-2K-39 reached 21.5 MPa, which is significantly higher than that of other flexible polysiloxane materials. Moreover, the tensile strength and breaking elongation of SiTPU-2K-39 were maintained at 80.9% and 94.6%, respectively, after three cycles of regeneration. The Si-TPUs prepared in this work may potentially be used in gas separation, medical materials, antifouling coatings, and other applications.

Keywords: polysiloxane-based; polyurethane; high strength; recyclability; microphase separation



Citation: Wang, W.; Bai, X.; Sun, S.; Gao, Y.; Li, F.; Hu, S.

Polysiloxane-Based Polyurethanes with High Strength and Recyclability.

Int. J. Mol. Sci. **2022**, *23*, 12613.

<https://doi.org/10.3390/ijms232012613>

ijms232012613

Academic Editor: Ana María Díez-Pascual

Received: 15 September 2022

Accepted: 15 October 2022

Published: 20 October 2022

Publisher's Note: MDPI stays neutral with regard to jurisdictional claims in published maps and institutional affiliations.



Copyright: © 2022 by the authors. Licensee MDPI, Basel, Switzerland. This article is an open access article distributed under the terms and conditions of the Creative Commons Attribution (CC BY) license (<https://creativecommons.org/licenses/by/4.0/>).

1. Introduction

Polysiloxanes possess a macromolecular backbone composed of repeating Si–O–Si bonds, with the direct attachment of organic groups to Si atoms. These materials are characterized by the excellent properties of both inorganic and organic materials [1–4]. The inorganic properties of Si materials effectively improve their heat resistance and flame retardancy [5], while their high Si–O–Si bond energy and low surface energy endow them with outstanding wear and weathering resistance [6]. In addition, polysiloxanes exhibit good hydrophobicity [7,8], high flexibility [9], and biocompatibility [10]. However, their low mechanical strength limits their applications in various fields [11,12].

The mechanical properties of polysiloxanes can be effectively improved by modification with other polymeric materials, such as epoxy resin [13], polyurea [14], polyether [15], and polyurethane [16]. Modification with polyurethane presents great significance as a modification technique because the molecule has a well-regulated structure. Polyurethanes are composed of alternating soft segments (SS) and hard segments (HS); SS confers flexibility and toughness, whereas HS provides rigidity, strength, wear resistance, and excellent mechanical properties [17–20]. Current methods to modify polysiloxanes using polyurethanes mainly include physical blending [21] and chemical copolymerization [22]. However, the solubility parameters of polyurethane and polysiloxane remarkably differ because of their different molecular structures; thus, these materials usually show poor

compatibility [23]. Modification by simple physical blending can lead to high interfacial tension and poor interfacial adhesion [24], resulting in macroscopic phase separation. In this case, polysiloxane easily migrates toward the surface of the blended material [25,26] because no chemical bonds are generated between polysiloxane and polyurethane. Thus, the stability of the modified Si polyurethane is poor, and the aging properties of the material are reduced. Modification by physical blending cannot meet the needs of most actual applications. Chemical modification involves the use of end-functionalized polysiloxanes for copolymerization with organic polymers to obtain new polymeric materials [27–29]. This technique fundamentally improves material compatibility and solves the drawbacks of physical blending [30–32].

Conventional polyurethane raw materials, such as polyether and polyester polyols, are petroleum-dependent products, which considerably limit their sustainable development [33–36]. The Earth's crust contains over 90 elements, with O and Si accounting for approximately 49% and 26% of the total abundance of these elements, respectively [37]. The utilization of Si resources can reduce energy consumption, improve the atmospheric environment, and realize sustainable economic development. Therefore, polysiloxane-based polyurethane materials have great development and application prospects. These modified materials can overcome the poor mechanical properties of polysiloxanes, rendering them applicable to textiles [38], medical materials [39–41], adhesives [42], and coatings [43–45], among others. Compared with aromatic isocyanates [46], aliphatic 4,4-dicyclohexylmethane diisocyanate (HMDI) and isophorone diisocyanate (IPDI) are ideal materials for synthesizing aliphatic polyurethanes for biomedical applications, owing to their nontoxicity and yellowing resistance [47–49]. Moreover, the water and heat resistances of HMDI-based TPU are better than those of IPDI-based TPUs. Therefore, in this study, HMDI was selected as the HS for synthesizing polyurethane.

In this work, hydroxyl-terminated polydimethylsiloxane (PDMS; HO–PDMS–OH) was selected to synthesize polysiloxane-based polyurethanes because amino-terminated PDMS (H₂N–PDMS–NH₂) reacts violently with isocyanate groups. However, HO–PDMS–OH is expensive, and the necessary technology is relatively immature when compared with the H₂N–PDMS–NH₂ approach; therefore, HO–PDMS–OH was presynthesized by reacting H₂N–PDMS–NH₂ and vinyl carbonate (EC), as described in our previous work [50]. Compared to conventional hydroxy silicone oil, the prepared OH–PDMS–OH possessed higher polarity and better compatibility with diisocyanates because of the I urethane groups. In addition, it could also increase hydrogen bond interactions, hence, improving mechanical properties [51]. Next, a series of polysiloxane-polyurethanes (Si-TPUs) was prepared by reacting HO–PDMS–OH, 4,4-dicyclohexylmethane diisocyanate (HMDI), and the chain extender 1,4-butanediol (BDO). The effects of SS number average molecular weight (M_n) and HS content on the microstructure and properties of the resultant Si-TPUs were evaluated. Overall, the prepared Si-TPUs exhibited good phase separation, excellent mechanical strength, and acceptable repeatable processability. Therefore, chemical copolymerization is a highly effective method for modifying polysiloxanes and can broaden their application areas.

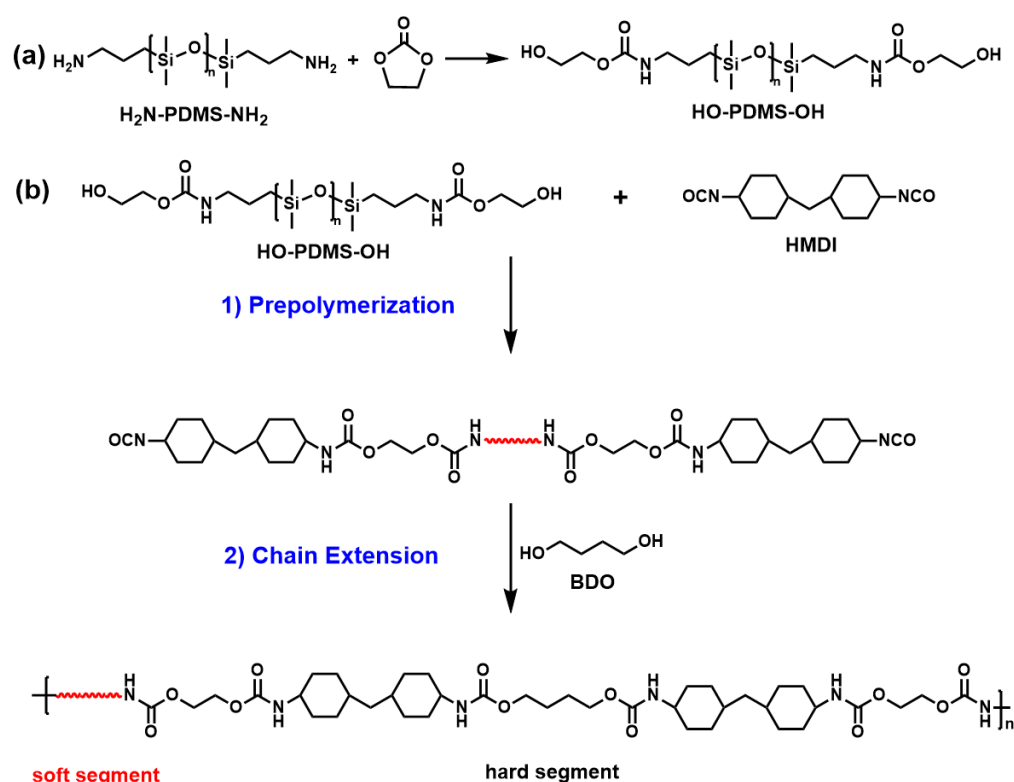
2. Experimental Section

2.1. Materials

Aminopropyl-terminated PDMS (H₂N–PDMS–NH₂, M_n = 1000, 2000, and 3000) was purchased from Beijing Warwick Chemical Co. Ltd. (Beijing, China). EC was obtained from Shanghai Adamas Reagent Co., Ltd. (Shanghai, China). Analytical-reagent-grade HMDI was obtained from Shanghai Macklin Biochemical Technology Co., Ltd. (Shanghai, China). Analytical-reagent-grade BDO was supplied by Shanghai Aladdin Biochemical Technology Co., Ltd. (Shanghai, China). Analytical-reagent-grade tetrahydrofuran (THF) was obtained from Beijing Chemical Works. Analytical-reagent-grade dibutyltin dilaurate (DBTL) was supplied by Hebei Bailing Weichao Fine Materials Co., Ltd. (Hebei, China).

2.2. Synthesis of the HMDI-Based Thermoplastic Polyurethanes

The SS HO-PDMS-OH was first prepared according to a previously described method [50]. Next, the HMDI-based Si-TPU was synthesized as follows. An oil bath was heated to 115 °C. A measured amount of HO-PDMS-OH (20 mmol) was then added to a three-necked flask equipped with a mechanical stirrer, nitrogen inlet, and condensate tube for 1.5 h of vacuum distillation. The temperature was reduced to 75 °C, and a measured amount of HMDI and two drops of the catalyst DBTL were added to the flask. The temperature was increased to 85 °C for prepolymerization and held for 2 h. Next, a measured amount of the chain extender BDO was introduced to the flask at 90 °C and mixed for 0.5 h. Finally, the obtained HMDI-based Si-TPU was poured into tetrafluoroethylene molds and cured for 12 h at 100 °C. The prepared Si-TPUs were denoted SiTPU-X-Y, where X represents the M_n value of SS and Y represents the HS content. The synthetic procedure is shown in Scheme 1, and the ratios of the raw materials are shown in Table 1.



Scheme 1. (a) Synthetic route of HO-PDMS-OH; (b) synthetic route of HMDI-based Si-TPUs.

Table 1. Chemical composition of the synthesized HMDI-based Si-TPUs.

| Sample | SS M_n | HS Content | PDMS:HMDI:BDO (Molar Ratio) |
|-------------|----------|------------|-----------------------------|
| SiTPU-1K-33 | 1000 | 33% | 1:1.15:0.15 |
| SiTPU-2K-19 | 2000 | 19% | 1:1.1:0.1 |
| SiTPU-2K-23 | 2000 | 23% | 1:1.45:0.45 |
| SiTPU-2K-28 | 2000 | 28% | 1:2:1 |
| SiTPU-2K-33 | 2000 | 33% | 1:2.5:1.5 |
| SiTPU-2K-39 | 2000 | 39% | 1:3.4:2.4 |
| SiTPU-3K-33 | 3000 | 33% | 1:4:3 |

2.3. Characterization

2.3.1. FT-IR Spectroscopy

FT-IR spectroscopy was performed on a Tensor 27 FT-IR spectrometer (Bruker, Bremen, Germany) under the following test conditions: test mode = ATR, wavenumber range = 500–4000 cm^{-1} , resolution = 4 cm^{-1} , and scanning number = 32.

2.3.2. Gel Permeation Chromatography (GPC)

GPC was performed using a Shimadzu GPC chromatograph (Kyoto, Japan). The Si-TPU samples were dissolved in THF and prepared into a solution of 10 mg/mL. The flow velocity was 1 mL/min. Polystyrene was used as the calibration standard.

2.3.3. Differential Scanning Calorimetry (DSC)

The DSC thermograms of the samples were measured on an STARe System DSC instrument (Mettler-Toledo, Greifensee, Switzerland). First, the temperature was reduced from 30 °C to −140 °C at a rate of −10 °C/min, and then maintained at this temperature for 10 min. The temperature was then increased to 100 °C at a rate of 10 °C/min under a continuous N_2 purge.

2.3.4. Wide-Angle X-ray Diffraction (WAXD)

WAXD spectra were recorded using a D/Max 2500 VB2+/PC model (Rigaku Corporation, Tokyo, Japan). The Si-TPU samples were prepared as flat flakes with a thickness of 1 mm at room temperature. Measurements were performed at a scanning rate of 5 °C/min in the 2θ range of 5–90°.

2.3.5. Small-Angle X-ray Scattering (SAXS)

SAXS measurements were performed on a Xues2-0 scatterer (Xenocs, Grenoble, France) at a wavelength of 0.154 nm. Herein, 2D SAXS patterns were acquired using a Pilatus 200 K detector. The distance between the detector and all samples, except SiTPU-1K-33, was 2490 mm; SiTPU-1K-33 was positioned at 1670 mm from the detector. The exposure time was set to 20 min.

2.3.6. Atomic Force Microscopy (AFM)

AFM measurements were performed using a Multimode 8 instrument (Bruker, Bremen, Germany) in tapping mode, with a scan area of $2 \times 2 \mu\text{m}^2$. The sample surface was polished well to enable precise measurements.

2.3.7. Tensile Testing

Tensile testing was performed using a Roell Tset-port II instrument (Zwick, Ulm, Germany) at room temperature. The strain rate was set to 50 mm/min. The mechanical properties of the Si-TPU products were tested using dumbbell-type flake splines with a thickness, width, and length of 1, 4, and 25 mm, respectively.

2.3.8. Repeatable Processability

The used samples were sheared into small pieces and molded into 1 mm films by a vulcanizer for reprocessing. The test conditions used to assess the repeatable processability of the samples were identical to those used to test their mechanical properties.

3. Results and Discussion

3.1. FT-IR Spectral Analysis

The chemical structures of the synthesized Si-TPUs were analyzed using FT-IR, as shown in Figure 1. The characteristic absorption peak of the NCO group in HMDI, which occurs at 2264 cm^{-1} , disappeared [52], indicating the complete reaction of this group. The characteristic peaks at 1708–1741 and 3322–3412 cm^{-1} correspond to the stretching vibrations of $-\text{C}=\text{O}$ and $-\text{NH}$, respectively. The stretching and asymmetric bending

vibrations of Si-CH₃ were observed at 1255–1261 and 791–812 cm⁻¹, respectively. The “M”-type peaks located at 1094–1097 and 1025–1028 cm⁻¹ are the characteristic absorption peaks of Si-O-Si. The peaks at 2961–2972 and 2932–2937 cm⁻¹ represent the asymmetric and symmetric stretching vibrations of -CH₂, respectively [15,21]. Thus, the FT-IR results confirmed the successful synthesis of the HMDI-based Si-TPUs.

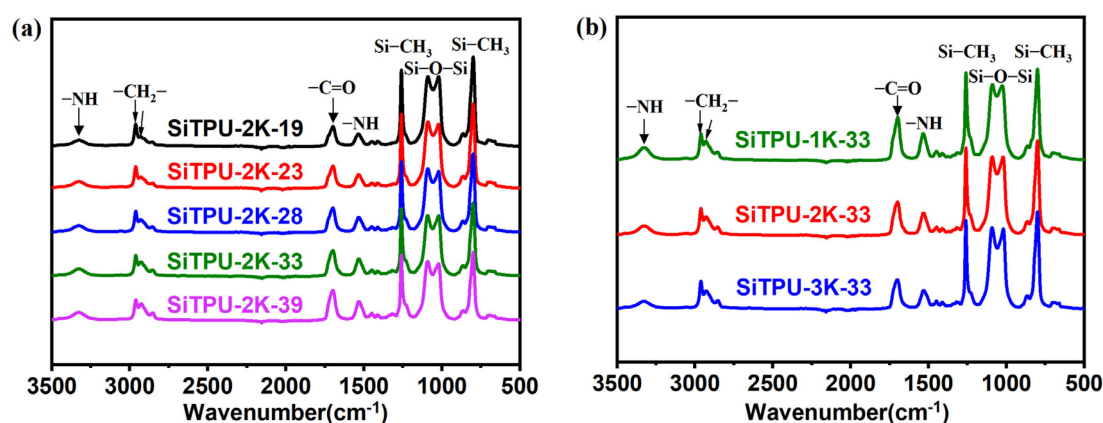


Figure 1. (a) FT-IR spectra of the Si-TPUs with different HS contents. (b) FT-IR spectra of the Si-TPUs with different M_n values of the SS.

The peaks in the carbonyl region from 1610 to 1800 cm⁻¹ could be resolved into two peaks at 1699 and 1726 cm⁻¹ (Figures S1 and S2), corresponding to hydrogen-bonded and free carbonyl groups, respectively [53]. Hydrogen bonding associations (HBA) are related to the proportion of carbonyl groups and can be calculated using the following formula [54]:

$$HBA = \frac{S_{1699}}{S_{1699} + S_{1726}} \times 100\%,$$

where S_{1699} represents the area of the hydrogen-bonded carbonyl peak at 1699 cm⁻¹ and S_{1726} represents the area of the free carbonyl peak at 1726 cm⁻¹. Table 2 lists the percentages of hydrogen-bonded and free carbonyl groups of the synthesized materials. As the HS content of the Si-TPUs increased, the proportion of hydrogen-bonded carbonyls increased and the proportion of free carbonyls decreased. These changes could be explained by the increase in number of hydrogen bonds formed between HS and separation of more HS from SS with increasing HS content. In addition, the proportion of hydrogen-bonded carbonyls decreased, whereas the proportion of free carbonyls increased as the SS M_n increased, possibly because of the increase in distance between carbamate groups, which decreases their density. Variable-temperature IR spectroscopy (Figure S3) indicated the dissociation of hydrogen bonds due to elevations in temperature. The proportion of hydrogen-bonded carbonyls and amino groups decreased, whereas that of free carbonyls and amino groups increased when the temperature was increased from 30 to 180 °C.

Table 2. Percentage of free and hydrogen-bonded carbonyl groups obtained from fitted-curve analysis.

| Sample | Hydrogen-Bonded Carbonyls (1699 cm ⁻¹) | Free Carbonyls (1726 cm ⁻¹) |
|-------------|--|---|
| SiTPU-1K-33 | 81.37 | 18.63 |
| SiTPU-2K-19 | 77.30 | 22.70 |
| SiTPU-2K-23 | 77.96 | 22.04 |
| SiTPU-2K-28 | 78.50 | 21.50 |
| SiTPU-2K-33 | 80.85 | 19.15 |
| SiTPU-2K-39 | 83.82 | 16.18 |
| SiTPU-3K-33 | 79.21 | 20.79 |

3.2. GPC

Figure 2 shows the GPC curves of the synthesized Si-TPUs, and Table S1 summarizes their molecular weights and molecular weight distributions (\bar{D}). The Si-TPU samples were dissolved in THF. The solutions completely passed through the filter membrane without insoluble particles, thus confirming the uncross-linked structure and high solubility of the synthesized HMDI-based Si-TPUs. The GPC results confirmed the relatively close values of M_n and average molecular weight (M_w), and all values obtained were greater than 25,000. The \bar{D} values of all compounds were approximately 1.9.

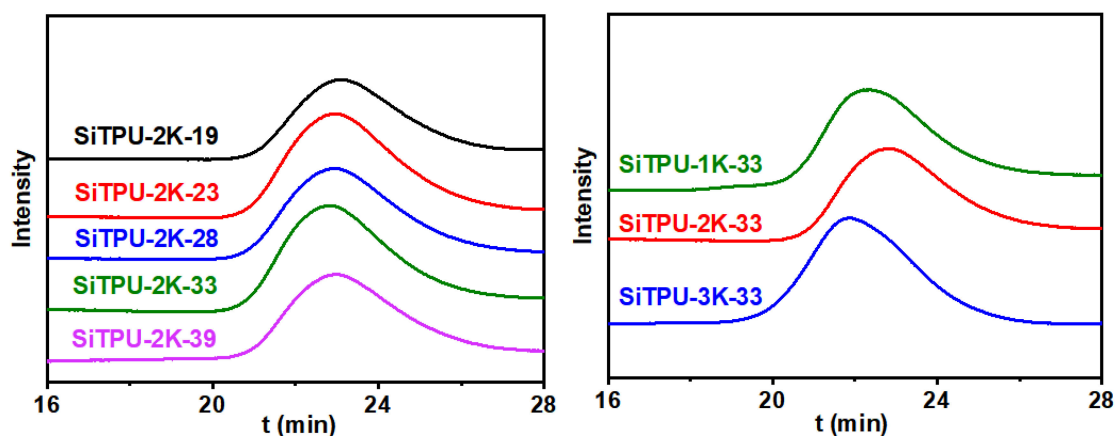


Figure 2. GPC curves of the HMDI-based Si-TPUs.

3.3. DSC

The DSC curves of Si-TPUs with different HS contents and SS M_n values are shown in Figure 3a,b, respectively. The Si-TPUs had two glass transition temperatures (T_g). T_{g1} , which is related to the SS and appeared at -123 °C, was barely influenced by the HS content and SS M_n value, whereas T_{g2} , which appeared at approximately 40 °C, was related to HS. As shown in Figure 3a, when the SS M_n was held constant, T_{g2} gradually increased as the HS content increased, mainly because the number of hydrogen bonds between HS increases with increasing HS content. However, the mobility of HS is limited. Thus, the energy required to move these segments increases, leading to a higher T_{g2} . As shown in Figure 3b, T_{g2} gradually increased with increasing SS M_n , mainly because the average HS M_n also increases as the SS M_n increases when the HS content is held constant. Increases in the number of hydrogen bonds between HS lead to a higher T_{g2} .

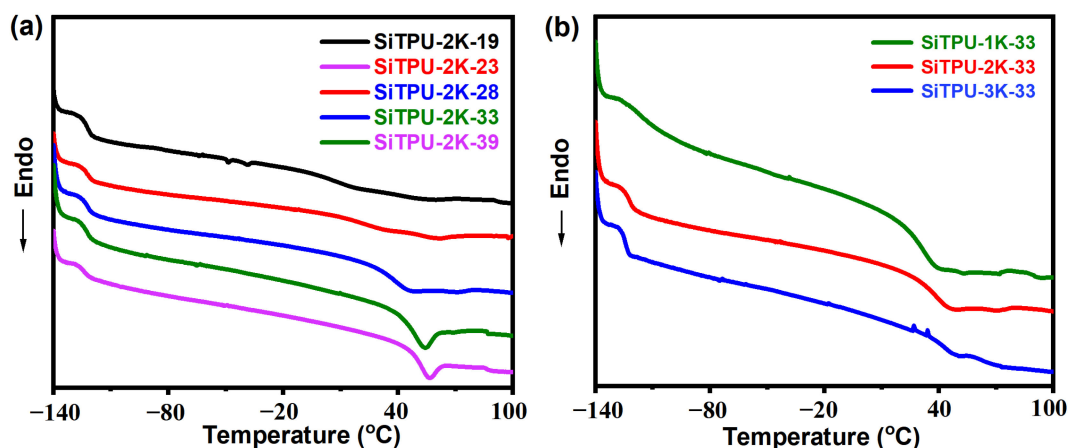


Figure 3. (a) DSC curves of the Si-TPUs with different HS contents (b) DSC curves of the Si-TPUs with different M_n values of the SS.

3.4. WAXD

Figure 4a,b show the 1D-WAXD curves of the prepared Si-TPUs. The broad diffusion peak at $2\theta = 12^\circ$ was assigned to the amorphous phase of PDMS, whereas that at 21° was assigned to the non-PDMS segments of the polymer chains [55,56]. Therefore, the SS and HS regions in the HMDI-based Si-TPUs similarly exhibited an amorphous morphology without sharp peaks.

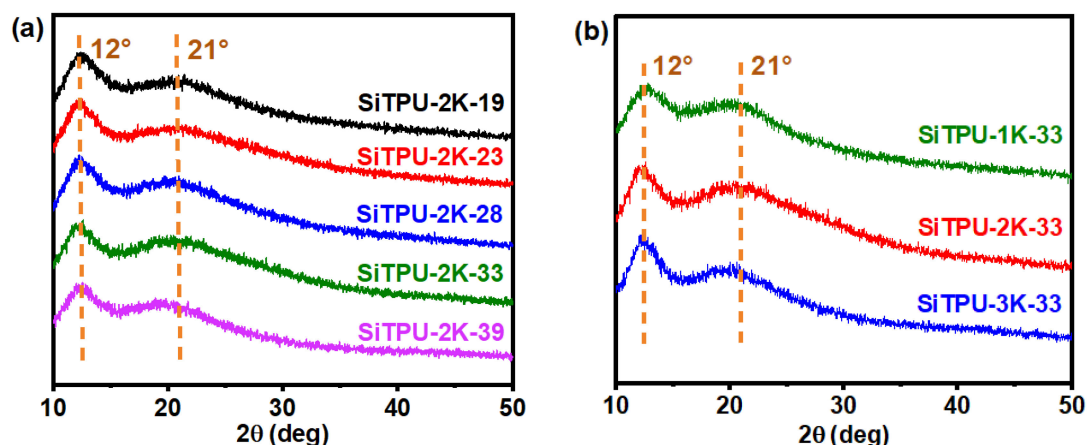


Figure 4. (a) WAXD curves of the Si-TPUs with different HS contents. (b) WAXD curves of the Si-TPUs with different M_n values of the SS.

3.5. SAXS

Figure 5a,b show the 1D-SAXS curves of the HMDI-based Si-TPUs with different HS contents and SS M_n values, respectively. Figure 5c shows the 2D-SAXS patterns of the Si-TPUs. The periodic sizes (D) of the synthesized materials are presented in Table S2. D reflects the mean distance between SS and HS regions and was calculated using the formula $D = 2\pi/q_{\max}$ [57,58], where q_{\max} represents the q value of the maximum scattering peak. The peaks and isotropic scattering rings shown in Figure 5 confirm that the HMDI-based Si-TPUs have microphase separation structures. Moreover, the scattering peak was gradually enhanced, the scattering loop became clearer, and D value increased as the HS content increased. These findings can be attributed to increases in HS average molecular weight and degree of phase separation with increasing HS content. Figure 5 and Table S2 show that q_{\max} gradually decreases, whereas D increases, as the SS M_n increases. In addition, the scattering peaks and loops are enhanced, mainly because the size of the SS microdomain and average HS M_n increase as the SS M_n increases. Thus, D and the degree of microphase separation increase accordingly, rendering the scattering peaks and rings more evident.

3.6. AFM

The microstructure of the Si-TPUs was investigated using tapping-mode AFM, as shown in Figure 6, to clarify their microphase separation structures. In the images obtained, the bright areas represent HS domains, whereas the dark areas represent SS domains. The AFM images reveal that the HS domains are evenly distributed in the SS phase and that the HMDI-based Si-TPUs exhibit excellent phase separation, which is consistent with the SAXS results. The AFM image of SiTPU-2K-39 reveals that the HS forms a continuous phase; moreover, the SS and HS domains are evenly distributed. By comparison, fewer HS domains are visible in the field of view of SiTPU-3K-33. The longer SS domains of SiTPU-3K-33 compared with those of SiTPU-1K-33 and SiTPU-2K-33 likely caused a reduction in the density of HS domains.

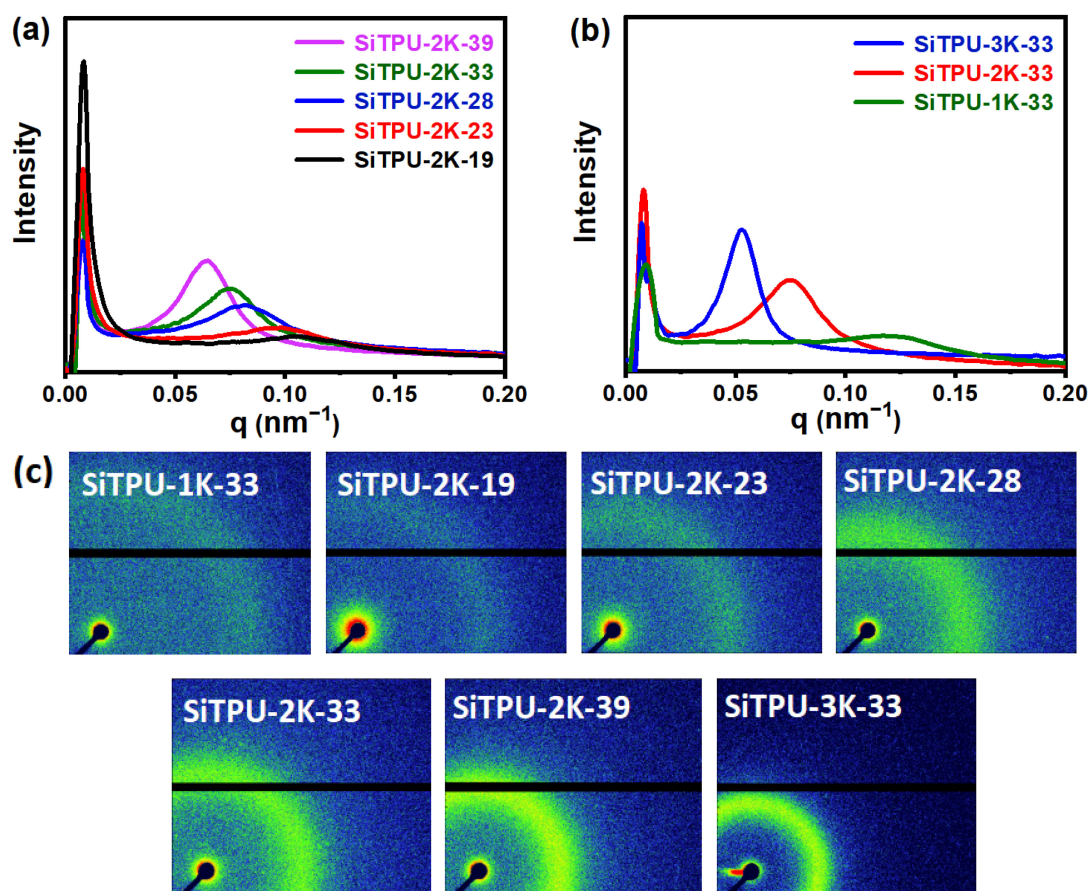


Figure 5. (a) 1D SAXS curves of Si-TPUs with different HS contents. (b) 1D SAXS curves of SiTPU-1K-33, SiTPU-2K-33, and SiTPU-3K-33. (c) 2D SAXS patterns of the HMDI-based Si-TPUs.

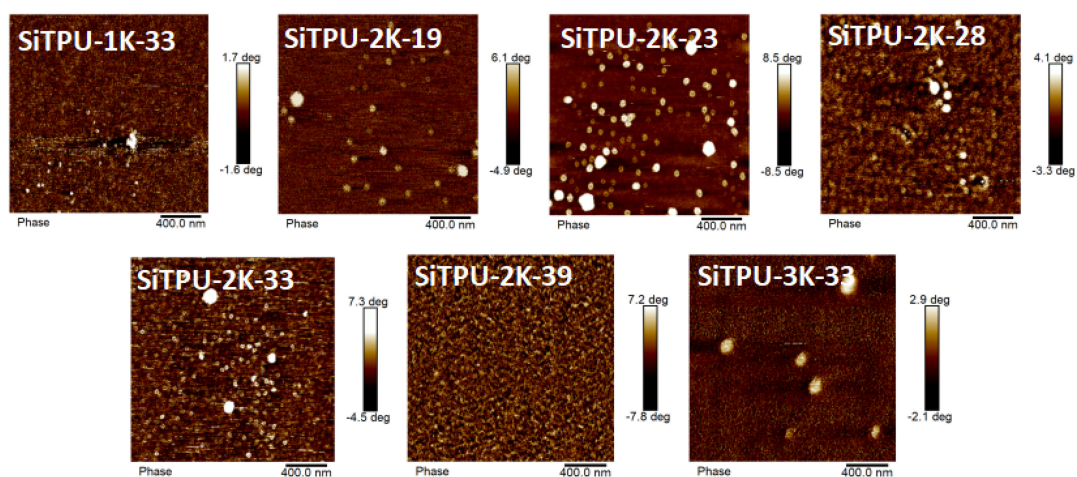


Figure 6. AFM images of the HMDI-based Si-TPUs.

3.7. Mechanical Properties

Curves of the various mechanical properties of the HMDI-based Si-TPUs are shown in Figure 7, and the detailed mechanical property data are listed in Table S3. As shown in Figure 7a,b, when the SS M_n was held constant, the tensile strength of the Si-TPUs increased significantly, whereas their breaking elongation decreased as the HS content increased. This finding may be attributed to the increase in number of hydrogen bonds and physical crosslinking points between polymer chains when the HS content is increased. Thus, the tensile strength of the Si-TPUs increased. However, excess physical crosslinking points

limit the slippage of polymer chains; therefore, the breaking elongation of the samples gradually decreased. As shown in Figure 7c,d, when the HS content was held constant, the elongation at break of the Si-TPUs decreased as the SS M_n increased, likely because the average length of the HS domains increases as the SS M_n increases. The number of hydrogen bonds also increases, thereby restricting the deformation of the materials. As the degree of physical crosslinking increases, the stress required to deform the materials uniformly increases; thus, their tensile stress at 100% breaking elongation increases. The ultimate tensile strength of SiTPU-1K-33 reached 17 MPa; such high strength could be attributed to the molecular orientation in the stretching direction and strain-induced crystallization during the stretching process [59,60]. These results collectively suggest that the HMDI-based Si-TPUs possess excellent mechanical properties.

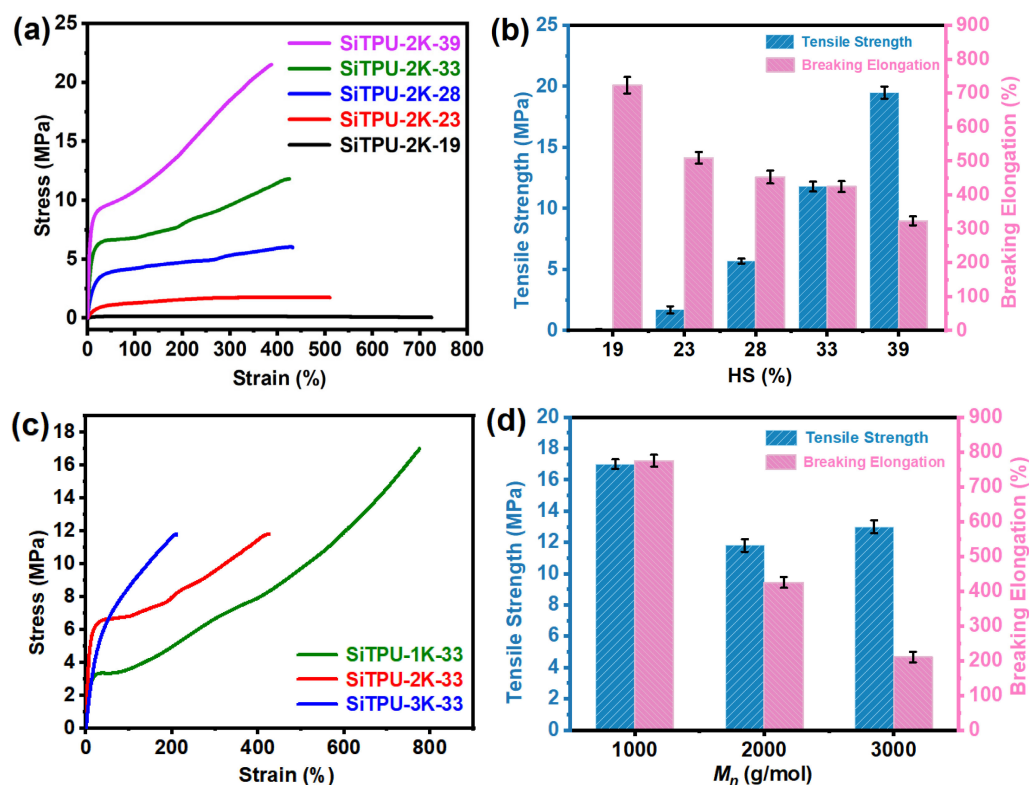


Figure 7. (a) Stress–strain curves of the Si-TPUs with different HS contents. (b) A histogram of mechanical properties of Si-TPUs with different HS contents. (c) Stress–strain curves of the Si-TPUs with different M_n values of the SS. (d) A histogram of mechanical properties of Si-TPUs with different M_n values of the SS.

3.8. Repeatable Processability

SiTPU-2K-39 had the highest tensile strength among the prepared Si-TPUs. Figure 8 presents its mechanical properties after three cycles of processing; the corresponding data are presented in Table S4. As shown in Figure 8, after three cycles of processing, the mechanical properties of SiTPU-2K-39 slightly decreased. The tensile strength of the sample decreased from 21.5 to 17.4 MPa, with a retention rate of 80.9%, and its elongation at break decreased from 388% to 367%, with a retention rate of 94.6%. The tensile stresses at 100% and 300% elongations were also slightly reduced. These changes may be mainly attributed to the generation of small molecular substances, which affect the mechanical properties of the sample, during repetitive processing. However, the sample maintained at least 80% of its original mechanical strength, indicating that the HMDI-based Si-TPUs have good repeatable processability.

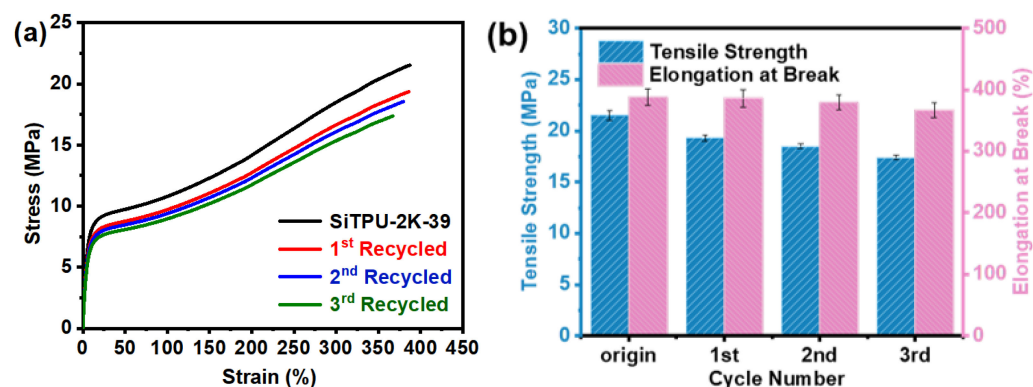


Figure 8. (a) Representative stress–strain curves of PDMS2K-39. (b) A histogram of mechanical properties of PDMS2K-39.

4. Conclusions

In this study, we successfully prepared thermoplastic HMDI-based Si-TPUs via a two-step reaction using HO-PDMS-OH, HMDI, and BDO. The Si-TPUs exhibited microphase separation, which influenced their mechanical properties, owing to the incompatibility between SS and HS. As the HS content increased, the tensile strength of the TPUs increased, whereas their breaking elongation decreased. When the HS content was held constant, the breaking elongation of the TPUs decreased with increasing SS M_n . The tensile strength of SiTPU-1K-33 reached 17.0 MPa. The mechanical properties of SiTPU-2K-39 were slightly degraded after three cycles of reprocessing. The tensile strength and breaking elongation of the sample were well maintained, with retention rates of 80.9% and 94.6%, respectively. These results demonstrate the good reusability and clear potential of the synthesized Si-TPUs for developing recycled materials. Overall, the block introduction of polysiloxanes into the polyurethane system by copolymerization can compensate for the individual deficiencies of these materials and enhance their comprehensive properties. Thus, Si-TPU-block copolymers are promising polymeric materials that can be widely utilized in various applications, such as biomedical materials, elastomers, functional coatings, and sealants.

Supplementary Materials: The following supporting information can be downloaded at: <https://www.mdpi.com/article/10.3390/ijms232012613/s1>. Figure S1. (a) FTIR spectra of Si-TPUs in the carbonyl regions from 1610 to 1800 cm^{-1} . Fitted Curve of the carbonyl groups of SiTPU-2K-19 (b), SiTPU-2K-23 (c), SiTPU-2K-28 (d), SiTPU-2K-33 (e) and SiTPU-2K-39 (f). Figure S2. (a) FTIR spectra of Si-TPUs in the carbonyl regions from 1610 to 1800 cm^{-1} . Fitted Curve of the carbonyl groups of SiTPU-1K-33 (b), SiTPU-2K-33 (c), SiTPU-3K-33 (d). Figure S3. FTIR spectra of (a) N–H and (b) C=O from SiTPU-2K-39. Table S1. Molecular weights and molecular weight distribution indices of Si-TPUs. Table S2. Periodic size (D) of the Si-TPUs. Table S3. Summary of the mechanical performance values of Si-TPUs. Table S4. The mechanical performance values of Si-TPUs after multiple recycles.

Author Contributions: Conceptualization, S.H. and W.W.; methodology, X.B. and S.S.; formal analysis, Y.G. and X.B.; data curation, X.B. and S.S.; writing—original draft preparation, W.W. and X.B.; writing—review and editing, S.H. and F.L.; funding acquisition, S.H. All authors have read and agreed to the published version of the manuscript.

Funding: This work was supported by the National Science Foundation for Young Scientists of China (No. 52203003).

Institutional Review Board Statement: Not applicable.

Informed Consent Statement: Not applicable.

Data Availability Statement: Not applicable.

Conflicts of Interest: The authors declare no conflict of interest.

References

1. Lipomi, D.J.; Bao, Z. Stretchable and ultraflexible organic electronics. *MRS Bull.* **2017**, *42*, 93–97. [[CrossRef](#)]
2. Zhou, J.; Wang, L.; Li, L.; Feng, S. Novel clickable and fluorescent poly (siloxane amine)s for reusable adhesives and reprocessable elastomers. *Polym. Chem.* **2020**, *11*, 4780–4786. [[CrossRef](#)]
3. Hu, H.; Wang, L.; Li, L.; Feng, S. Imine-functionalized polysiloxanes for supramolecular elastomers with tunable mechanical properties. *Polym. Chem.* **2020**, *11*, 7721–7728. [[CrossRef](#)]
4. Sun, Z.; Huang, S.; Wu, J.; Zhang, Q. Facile fabrication of superhydrophobic coating based on polysiloxane emulsion. *Prog. Org. Coat.* **2017**, *102*, 131–137. [[CrossRef](#)]
5. Cui, Y.; Pan, H.; Zhang, J.; Cao, L.; Zong, C. Influence of polydimethylsiloxane on the microstructure and properties of polyester thermoplastic polyurethane. *J. Polym. Res.* **2022**, *29*, 218. [[CrossRef](#)]
6. Zhao, Z.; Ju, P.; Ji, L.; Chen, L.; Wu, Y.; Zhou, H.; Chen, J. Structure optimization of epoxy-functionalized polysiloxanes and tribological properties of the polysiloxane/molybdenum disulfide lubricating coating for low-earth orbit environment. *Tribol. Int.* **2021**, *162*, 107135. [[CrossRef](#)]
7. Qiao, M.; Xu, W.; Ji, G.; Zhang, B. Anti-corrosion, anti-bacterial and durable atmospheric weatherability of polydimethylsiloxane coating with intrinsic hydrophobicity. *Surf. Topogr. Metrol. Prop.* **2022**, *10*, 025009. [[CrossRef](#)]
8. Dhali, K.; Daver, F.; Cass, P.; Adhikari, B. Surface modification of the cellulose nanocrystals through vinyl silane grafting. *Int. J. Biol. Macromol.* **2022**, *200*, 397–408. [[CrossRef](#)]
9. Mihara, S.; Takeok, S. Preparation and characterization of highly elongated polydimethylsiloxane nanosheets. *Polym. Advan. Technol.* **2022**, *33*, 1180–1189. [[CrossRef](#)]
10. Meng, Y.; Xu, W.; Newman, M.R.; Benoit, D.S.W.; Anthamatten, M. Thermoreversible siloxane networks: Soft biomaterials with widely tunable viscoelasticity. *Adv. Funct. Mater.* **2019**, *29*, 1903721. [[CrossRef](#)]
11. Berahman, R.; Raiati, M.; Mazidi, M.M.; Paran, S.M.R. Preparation and characterization of vulcanized silicone rubber/halloysite nanotube nanocomposites: Effect of matrix hardness and HNT content. *Mater. Des.* **2016**, *104*, 333–345. [[CrossRef](#)]
12. Xu, Q.; Pang, M.; Zhu, L.; Zhang, Y.; Feng, S. Mechanical properties of silicone rubber composed of diverse vinyl content silicone gums blending. *Mater. Des.* **2010**, *31*, 4083–4087. [[CrossRef](#)]
13. Sun, X.; Chen, R.; Gao, X.; Liu, Q.; Liu, J.; Zhang, H.; Yu, J.; Liu, P.; Takahashi, K.; Wang, J. Fabrication of epoxy modified polysiloxane with enhanced mechanical properties for marine antifouling application. *Eur. Polym. J.* **2019**, *117*, 77–85. [[CrossRef](#)]
14. Sirrine, J.M.; Schexnayder, S.A.; Dennis, J.M.; Long, T.E. Urea as a monomer for isocyanate-free synthesis of segmented poly(dimethyl siloxane) polyureas. *Polymer* **2018**, *154*, 225–232. [[CrossRef](#)]
15. Fang, P.; Bai, Y.; Wang, W.; Ma, X.; Tai, X.; Wang, G. Properties of ABA and BA polysiloxane amphiphiles modified by polyether. *J. Dispers. Sci. Technol.* **2018**, *39*, 1010–1017. [[CrossRef](#)]
16. Xu, C.-A.; Chen, G.; Tan, Z.; Hu, Z.; Qu, Z.; Zhang, Q.; Lu, M.; Wu, K.; Lu, M.; Liang, L. Evaluation of cytotoxicity in vitro and properties of polysiloxane-based polyurethane/lignin elastomers. *React. Funct. Polym.* **2020**, *149*, 104514. [[CrossRef](#)]
17. Hu, S.; He, S.; Wang, Y.; Wu, Y.; Shou, T.; Yin, D.; Mu, G.; Zhao, X.; Gao, Y.; Liu, J.; et al. Self-repairable, recyclable and heat-resistant polyurethane for high-performance automobile tires. *Nano Energy* **2022**, *95*, 107012. [[CrossRef](#)]
18. Zhao, X.; Fu, G.; Wang, Y.; Wu, Y.; Shou, T.; Yin, D.; Li, X.; Hu, S.; Zhang, L. Bio-based polyurethane/hindered phenol AO-80 composites for room temperature high damping properties. *Compos. Part B Eng.* **2022**, *243*, 110118. [[CrossRef](#)]
19. Francolini, I.; Silvestro, I.; di Lisio, V.; Martinelli, A.; Piozziet, A. Synthesis, characterization, and bacterial fouling-resistance properties of polyethylene glycol-grafted polyurethane elastomers. *Int. J. Mol. Sci.* **2019**, *20*, 1001. [[CrossRef](#)] [[PubMed](#)]
20. Rapone, I.; Taresco, V.; Lisio, V.; Piozzi, A.; Francolini, I. Silver- and Zinc-Decorated Polyurethane Ionomers with Tunable Hard/Soft Phase Segregation. *Int. J. Mol. Sci.* **2021**, *22*, 6134. [[CrossRef](#)] [[PubMed](#)]
21. Kilic, N.T.; Can, B.N.; Kodal, M.; Özkoç, G. Reactive compatibilization of biodegradable PLA/TPU blends via hybrid nanoparticle. *Prog. Rubber Plast. Recycl. Technol.* **2021**, *37*, 301–326. [[CrossRef](#)]
22. Zhu, R.; Wang, X.; Yang, J.; Wang, Y.; Zhang, Z.; Hou, Y.; Lin, F. Influence of hydroxyl-terminated polydimethylsiloxane on high-strength biocompatible polycarbonate urethane films. *Biomed. Mater.* **2016**, *12*, 015011. [[CrossRef](#)]
23. Uchida, T.; Kawaguchi, S.; Ito, K. Dispersion (co)polymerization of styrene in polymeric media to prepare polymer micro blends. *Des. Monomers Polym.* **2002**, *5*, 285–296. [[CrossRef](#)]
24. Hu, J.; Song, Y.; Ning, N.; Zhang, L.; Yu, B.; Tian, M. An effective strategy for improving the interface adhesion of the immiscible methyl vinyl silicone elastomer/thermoplastic polyurethane blends via developing a hybrid janus particle with amphiphilic brush. *Polymer* **2021**, *214*, 123375. [[CrossRef](#)]
25. Gordin, C.; Delaite, C.; Bistac, S.; Schuller, A.S.; Rusu, D.; Rusu, M. PDMS migration at poly (vinyl chloride)/poly (ϵ -caprolactone)/poly (ϵ -caprolactone)-b-poly (dimethylsiloxane) blends surfaces. *Polym. Test.* **2009**, *28*, 446–451. [[CrossRef](#)]
26. Zhang, Q.; Wu, M. Structure of vinyl polysiloxane on properties of polyacrylates film and its pigment printing application. *J. Coat. Technol. Res.* **2020**, *17*, 937–948. [[CrossRef](#)]
27. Zhao, R.; Zhang, Z.; Qi, Y. Influence of Epoxy Content on the Properties and Marine Bacterial Adhesion of Epoxy Modified Silicone Coatings. *Coatings* **2020**, *10*, 126. [[CrossRef](#)]
28. Qian, Y.; Dong, F.; Guo, L.; Xu, X.; Liu, H. Two-component waterborne polyurethane modified with terpene derivative-based polysiloxane for coatings via a thiol-ene click reaction. *Ind. Crop. Prod.* **2021**, *171*, 113903. [[CrossRef](#)]

29. Zuo, M.; Jiang, Z.; Guo, L.; Dong, F.; Guo, J.; Xu, X. Using α -Pinene-Modified Triethoxysilane as the New Cross-Linking Agent To Improve the Silicone Rubber Properties. *ACS Omega* **2019**, *4*, 11921–11927. [[CrossRef](#)]
30. Cui, Y.; Xu, Z.; Li, Y.; Lang, X.; Zong, C.; Cao, L. Synergistic thermodynamic compatibility of polydimethylsiloxane block in thermoplastic polyurethane for flame retardant materials: Super flexible, highly flame retardant and low smoke release. *Polymer* **2022**, *253*, 124976. [[CrossRef](#)]
31. Cui, Y.; Pan, H.; Shi, C.; Zhuang, H.; Wang, Q.; Zong, C. A method to essentially increase the compatibility of thermoplastic polyurethane/methyl vinyl silicone rubber based thermoplastic vulcanizate. *J. Appl. Polym. Sci.* **2022**, *139*, 52219. [[CrossRef](#)]
32. Cui, Y.; Yan, T.; Pan, H.; Sun, H.; Bai, X.; Cao, L.; Zong, C. Preparation and Characterization of Intrinsically Compatibilized Thermoplastic Polyurethane and Silicone Rubber. *Macromol. Chem. Phys.* **2022**, *223*, 2270018. [[CrossRef](#)]
33. Vale, M.; Mateus, M.M.; Santos, R.G.d.; de Castro, C.N.; de Schrijver, A. Replacement of petroleum-derived diols by sustainable biopolyols in one component polyurethane foams. *J. Clean. Prod.* **2019**, *212*, 1036–1043. [[CrossRef](#)]
34. Cefarin, N.; Bedolla, D.E.; Surowka, A.; Donato, S.; Sepperer, T.; Tondi, G.; Dreossi, D.; Sodini, N.; Birarda, G.; Vaccari, L. Study of the Spatio-Chemical Heterogeneity of Tannin-Furanic Foams: From 1D FTIR Spectroscopy to 3D FTIR Micro-Computed Tomography. *Int. J. Mol. Sci.* **2021**, *22*, 12869. [[CrossRef](#)]
35. Liu, F.; Chen, S. The Preparation and Characterization of Polyurethane Foam with Coconut Oil Polyol and Rapeseed Oil Polyol. *J. Polym. Environ.* **2021**, *29*, 2421–2434. [[CrossRef](#)]
36. Yang, W.; Han, Y.; Zhang, W.; Zhang, D. High-Strength and Low-Cost Biobased Polyurethane Foam Composites Enhanced by Poplar Wood Powder Liquefaction. *Polymers* **2021**, *13*, 2999. [[CrossRef](#)]
37. Kucinska-Lipka, J.; Gubanska, I.; Strankowski, M.; Ciesliński, H.; Filipowicz, N.; Janik, H. Synthesis and characterization of cycloaliphatic hydrophilic polyurethanes, modified with l -ascorbic acid, as materials for soft tissue regeneration. *Mater. Sci. Eng. C* **2017**, *75*, 671–681. [[CrossRef](#)]
38. Lei, W.; Sun, Y.; Huang, B.; Zhou, X. Synthesis and Application of Polyurethane-Modified Silicone as Finishing Agent for Cotton Fabric. *Fibers Polym.* **2018**, *19*, 1024–1031. [[CrossRef](#)]
39. Sharma, S.; Mandhani, A.; Bose, S.; Basu, B. Dynamically crosslinked polydimethylsiloxane-based polyurethanes with contact-killing antimicrobial properties as implantable alloplasts for urological reconstruction. *Acta Biomater.* **2021**, *129*, 122–137. [[CrossRef](#)]
40. Al Kayal, T.; Losi, P.; Asaro, M.; Volpi, S.; Bonani, W.; Bonini, M.; Soldani, G. Analysis of oxidative degradation and calcification behavior of a silicone polycarbonate polyurethane-polydimethylsiloxane material. *J. Biomed. Mater. Res. Part A* **2022**, *110*, 1109–1120. [[CrossRef](#)]
41. Noreen, A.; Zia, K.M.; Tabasum, S.; Aftab, W.; Shahid, M.; Zuber, M. Structural elucidation and biological aptitude of modified hydroxyethylcellulose-polydimethyl siloxane based polyurethanes. *Int. J. Biol. Macromol.* **2020**, *150*, 426–440. [[CrossRef](#)] [[PubMed](#)]
42. Dores, A.P.D.; Llorente, O.; Martin, L.; González, A.; Irusta, L. Polydimethylsiloxane containing waterborne hydrophobic polyurethane coatings with good adhesion to metals: Synthesis and characterization. *Prog. Org. Coat.* **2022**, *162*, 106564. [[CrossRef](#)]
43. Galhenage, T.P.; Hoffman, D.; Silbert, S.D.; Stafslie, S.J.; Daniels, J.; Miljkovic, T.; Finlay, J.A.; Franco, S.C.; Clare, A.S.; Nedved, B.; et al. Fouling-Release Performance of Silicone Oil-Modified Siloxane-Polyurethane Coatings. *ACS Appl. Mater. Interfaces* **2016**, *8*, 29025–29036. [[CrossRef](#)] [[PubMed](#)]
44. Galhenage, T.P.; Stafslie, S.J.; Skaja, A.; Webster, D.C. Durable siloxane-polyurethane coatings for mitigating freshwater mussel fouling. *Biofouling* **2022**, *38*, 260–270. [[CrossRef](#)]
45. Kim, M.G.; Jo, K.I.; Kim, E.; Park, J.H.; Ko, J.W.; Lee, J.H. Preparation of Polydimethylsiloxane-Modified Waterborne Polyurethane Coatings for Marine Applications. *Polymers* **2021**, *13*, 4283. [[CrossRef](#)]
46. Hu, S.; Wu, Y.; Fu, G.; Shou, T.; Zhai, M.; Yin, D.; Zhao, X. Bio-Based Polyurethane and Its Composites towards High Damping Properties. *Int. J. Mol. Sci.* **2022**, *23*, 6618. [[CrossRef](#)]
47. Byrne, C.A.; Mack, D.P.; Sloan, J.M. A Study of Aliphatic Polyurethane Elastomers Prepared from Diisocyanate Isomer Mixtures. *Rubber Chem. Technol.* **1985**, *58*, 985–996. [[CrossRef](#)]
48. Lee, D.-K.; Tsai, H.-B. Properties of segmented polyurethanes derived from different diisocyanates. *J. Appl. Polym. Sci.* **2000**, *75*, 167–174. [[CrossRef](#)]
49. Cheng, Q.; Zheng, Y.; Wang, T.; Sun, D.; Lin, R. Yellow resistant photosensitive resin for digital light processing 3D printing. *J. Appl. Polym. Sci.* **2020**, *137*, 48369. [[CrossRef](#)]
50. Wang, W.; Sun, S.; Hu, S.; Yang, B.; He, S.; Wang, R.; Zhang, L. Unprecedented Strength Polysiloxane-Based Polyurethane for 3D Printing and Shape Memory. *ACS Appl. Mater. Interfaces* **2022**, *14*, 3324–3333. [[CrossRef](#)]
51. Sun, N.; Di, M.; Liu, Y. Lignin-containing polyurethane elastomers with enhanced mechanical properties via hydrogen bond interactions. *Int. J. Biol. Macromol.* **2021**, *184*, 1–8. [[CrossRef](#)]
52. Xu, C.-A.; Qu, Z.; Tan, Z.; Nan, B.; Meng, H.; Wu, K.; Shi, J.; Lu, M.; Liang, L. High-temperature resistance and hydrophobic polysiloxane-based polyurethane films with cross-linked structure prepared by the sol-gel process. *Polym. Test.* **2020**, *86*, 106485. [[CrossRef](#)]
53. Hu, S.; Shou, T.; Fu, G.; Zhao, X.; Wang, Z.; Zhang, L. New Stratagem for Designing High-Performance Thermoplastic Polyurethane by Using a New Chain Extender. *Macromol. Chem. Phys.* **2021**, *222*, 2000439. [[CrossRef](#)]

54. Kong, Z.; Tian, Q.; Zhang, R.; Yin, J.; Shi, L.; Bin Ying, W.; Hu, H.; Yao, C.; Wang, K.; Zhu, J. Reexamination of the microphase separation in MDI and PTMG based polyurethane: Fast and continuous association/dissociation processes of hydrogen bonding. *Polymer* **2019**, *185*, 121943. [[CrossRef](#)]
55. Choi, T.; Weksler, J.; Padsalgikar, A.; Runt, J. Microstructural organization of polydimethylsiloxane soft segment polyurethanes derived from a single macrodiol. *Polymer* **2010**, *51*, 4375–4382. [[CrossRef](#)]
56. Hernandez, R.; Weksler, J.; Padsalgikar, A.; Runt, J. Microstructural Organization of Three-Phase Polydimethylsiloxane-Based Segmented Polyurethanes. *Macromolecules* **2007**, *40*, 5441–5449. [[CrossRef](#)]
57. Hu, S.; Shou, T.; Zhao, X.; Wang, Z.; Zhang, S.; Qin, X.; Guo, M.; Zhang, L. Rational design of a novel NDI-based thermoplastic polyurethane elastomer with superior heat resistance. *Polymer* **2020**, *205*, 122764. [[CrossRef](#)]
58. Tang, L.; Shao, S.; Wang, A.; Tian, C.; Luo, F.; Li, J.; Li, Z.; Tan, H.; Zhang, H. Influence of fluorocarbon side chain on microphase separation and chemical stability of silicon-containing polycarbonate urethane. *Polymer* **2022**, *242*, 124538. [[CrossRef](#)]
59. Wang, F.; Chen, S.; Wu, Q.; Zhang, R.; Sun, P. Strain-induced structural and dynamic changes in segmented polyurethane elastomers. *Polymer* **2019**, *163*, 154–161. [[CrossRef](#)]
60. Xu, C.; Ding, S.; Liu, X.; Wang, F.; Shi, Y.; Wang, X.; Wang, Z. Superhigh strength polyurethane materials with oriented microdomains produced through mechanical deformation. *Polymer* **2022**, *253*, 124968. [[CrossRef](#)]